Isotopic yields of intermediate-mass fragments emitted in $E/A = 50$ MeV ^{4}He + ^{116,124}Sn reactions

J. Brzychczyk,* D. S. Bracken, K. Kwiatkowski, K. B. Morley, E. Renshaw, and V. E. Viola
Departments of Chemistry and Physics and Indiana University Cyclotron Facility, Indiana University, Bloomington, Indiana 47405
(Received 13 October 1992)

Inclusive yields of isotopically resolved intermediate-mass fragments (IMF) with $Z = 3-6$ have been measured for the reaction of $E/A = 50$ MeV ^{4}He with ^{116}Sn and ^{124}Sn targets. The isotopic yield patterns reflect the N/Z ratio of the target for both equilibriumlike and nonequilibrium components of the spectra. In addition, the IMF elemental cross sections for the ^{124}Sn target decrease much more rapidly with Z than for ^{116}Sn. This effect is presumably due to lower barriers for IMF emission from residues formed with the neutron-deficient ^{116}Sn target and increased competition from pre-IMF neutron emission for the neutron-excess ^{124}Sn target. The experimental cross sections are compared with statistical and accreting-source calculations.

PACS number(s): 25.70.Mn

I. INTRODUCTION

Inclusive studies of intermediate-mass fragments (IMF: $3 \leq Z \leq 15$) have provided valuable insight into the nature of both the reaction dynamics and decay mechanisms which characterize intermediate-energy nucleus-nucleus collisions [1–7]. The systematic evolution of IMF kinetic energy, angular, and charge distributions as a function of projectile energy has demonstrated that IMF emission occurs over a wide range of interaction times—extending from fast nonequilibrium mechanisms to time scales characteristic of fully equilibrated compound nuclei [8]. The data support a picture in which the emission time scale becomes shorter as a function of increasing impact parameter and bombarding energy, a conclusion reinforced by recent exclusive studies [9,10].

While most of the existing inclusive data are for charge- (or mass-) identified fragments, discrete isotopic yield information has further enriched our understanding of IMF emission mechanisms [1,11–15]. Relative isotopic yields for a given element have been shown to reflect the N/Z composition of the emitting source [11]. This result has important implications for the mechanism of nonequilibrium IMF emission—as yet poorly understood—in that the neutron-excess character of the ejectiles implies formation from a composite source, rather than a projectilelike peripheral interaction [8]. The isotopic ratios also evolve as a function of fragment kinetic energy; neutron-excess fragments are favored for low-energy ejectiles, whereas neutron deficient species are more abundant in the high-energy tails of the spectra (dependent somewhat on ejectile mass and angle of observation). Hence, slope temperatures derived from elemental spectra, which represent an average over all isotopes, must be interpreted with caution. Wada *et al.* [11] have also used isotope-ratio data to infer the relation between the nuclear density and temperature at breakup. Qualitative success has been obtained in describing isotopic ratio data with an accreting source model [14,16] and a statistical fragmentation model [12,17].

In the present work we investigate the influence of target N/Z ratio on the properties of IMFs formed in the reaction of $E/A \approx 50$ MeV ^{4}He ions with targets of ^{116}Sn ($N/Z = 1.32$) and ^{124}Sn ($N/Z = 1.48$). The use of light-ion projectiles eliminates contributions due to projectile fragmentation, thus permitting a more direct comparison between equilibrium and nonequilibrium targetlike sources.

II. EXPERIMENTAL DETAILS

The experiment was performed at the Indiana University Cyclotron Facility with ^{4}He beams of 180 and 200 MeV incident energy. Self-supporting ^{116}Sn and ^{124}Sn targets were used, each with areal densities of 1.4 mg/cm^2 and isotopic purity of 95.6% and 96.7%, respectively.

Reaction products ($Z \geq 3$) were detected with two telescopes positioned on rotatable arms inside a 162-cm-diam scattering chamber. The first telescope, employed primarily at forward angles, consisted of an axial-field gas-ionization chamber followed by 90 μm and 1 mm silicon surface-barrier detectors (450 mm^2), and a 2-cm-thick CsI(Tl) scintillator crystal readout with a photodiode. The first silicon element was placed 38 cm from the target and was also used for timing, with the beam rf signal as the time reference. Time-of-flight (TOF) and ΔE-E measurements provided low energy thresholds and full isotope separation for $Z \leq 6$ fragments. The second telescope consisted of a gas-ionization chamber followed by a 500 μm passivated silicon detector (25 cm^2) [18]. The 6.2 cm active length gas-ionization chambers were operated at 20 Torr of CF_4. Inclusive energy spectra of the intermediate mass fragments were measured with the ΔE-E/TOF telescope at forward angles of 12°, 35°, and 65°, and with the large solid-angle ΔE-E telescope at 160°. The TOF/ΔE-E telescope was also used to perform complementary measurements at the backward angle. This measurement was performed at 154° and 180 MeV

*Permanent address: Institute of Physics, Jagellonian University, Reymonta 4, 31-059, Krakow, Poland.

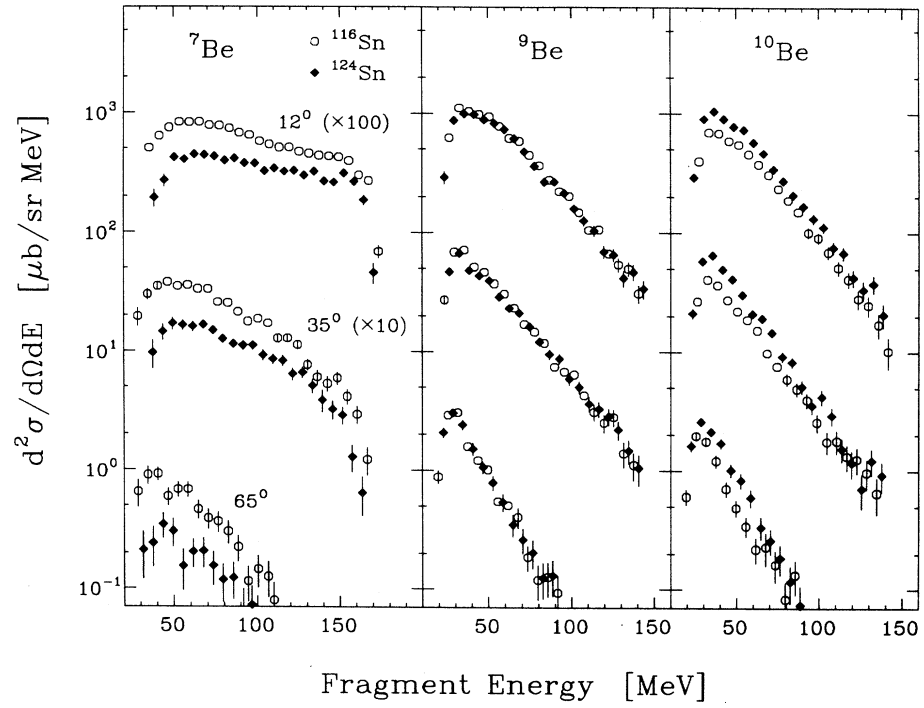

FIG. 1. Spectra for Be fragments measured at 12°, 35°, and 65° for ^{116}Sn (open points) and ^{124}Sn targets (closed points), as indicated on figure. Cross sections have been multiplied by factors indicated on figure.

incident energy. For both systems fragment kinetic-energy thresholds were $E/A \simeq 0.4$ MeV.

Runs with a blank target frame and a Mylar target were carried out to evaluate contamination of the spectra from beam halo and/or impurities in the targets. The low-energy part of the spectrum just above the instrumental threshold was well separated from the peak corresponding to the Coulomb energy for a given Z fragment emitted from a targetlike nucleus. Contamination from light-element impurities in the target was subtracted using energy spectra measured with the Mylar target. The uncertainties associated with this procedure are included in the quoted errors of the data.

The detectors were calibrated using an ^{241}Am alpha source and a precision pulse generator; the DONNA program [19] was used to calculate energy losses in the target and detector windows. Absolute cross sections were determined from the measured target thickness, known detector geometry, and integrated beam current, corrected for electronic and computer deadtimes. Data were acquired with standard NIM and CAMAC electronics, an Microprogramable Branch Driver (MBD), and a VAX 11/750 computer. A light-ion software rejection procedure was incorporated into the XSYS program [20] controlling data acquisition.

III. RESULTS

Figure 1 shows the energy spectra of Be isotopes at several angles from ^{116}Sn and ^{124}Sn targets. Spectra are corrected for contamination using the subtraction procedure described in Sec. II. Energy spectra for ^{7}Be at 12° and 35° exhibit significant contributions from nonequilibrium processes in the high-energy tails; ^{6}Li and ^{7}Li behave similarly. Spectra of ^{9}Be and ^{10}Be are representative of $A \geq 9$ fragments, and the spectral shapes are similar for both targets. As has been reported previously for a similar system [3], the high-energy tail becomes steeper at larger angles and for higher Z fragments. The qualita-

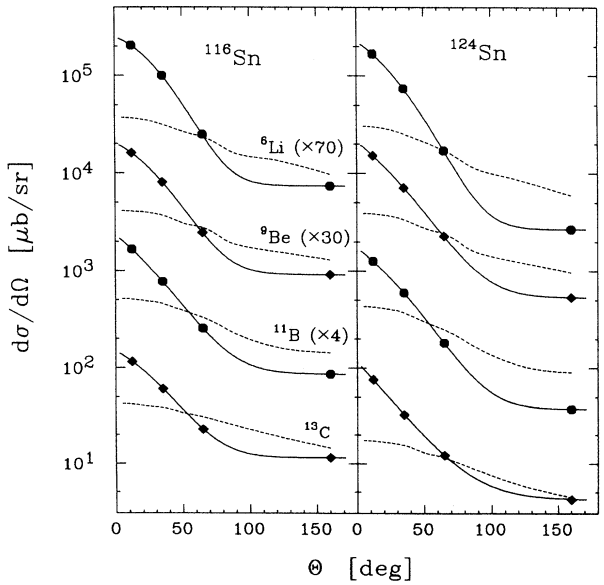

FIG. 2. Angular distributions of ^{6}Li, ^{9}Be, ^{11}B, and ^{13}C isotopes from ^{116}Sn (left) and ^{124}Sn (right) targets. Solid line is fit to data using Eq. (1). Cross sections have been multiplied by factors indicated on figure. Dashed line is accreting source fit [16,31].

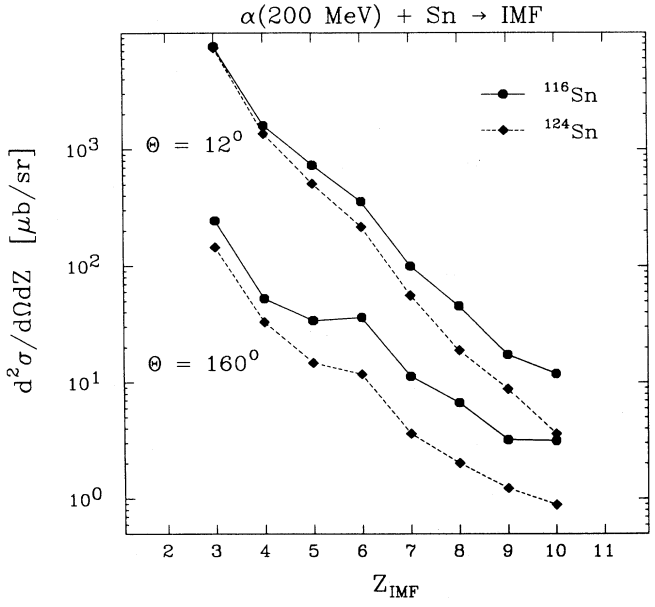

FIG. 3. Charge distributions at 12° (upper set) and 160° (lower set) for IMFs emitted from ^{116}Sn (solid lines) and ^{124}Sn (dotted lines).

tive dependence of IMF yield on target N/Z is apparent in Fig. 1. Neutron-deficient ^{7}Be is produced with much higher probability from ^{116}Sn than from ^{124}Sn, whereas the reverse is true for neutron-rich ^{10}Be. For beta-stable ^{9}Be, the yields are nearly identical for both targets. In addition, the spectral slopes exhibited by each of the Be isotopes differ dramatically. This fact can influence the "slope temperatures" derived from Maxwellian fits to elemental yields, since the result may be dependent on the isotopic composition for a given Z fragment.

Representative angular distributions are shown in Fig. 2. The data are fitted with a functional form

$$\frac{d\sigma}{d\Omega}(\theta) = \exp(a\theta^2 + b\theta + c) + d \ , \quad (1)$$

given by the solid lines in the figure. This parameterization has been used to calculate total cross sections for each nuclide. (See Table I.) It was assumed that the relative isotopic yields (isotope/element) measured at 160° in the 200 MeV bombardments are the same as those measured with the 180 MeV beam at 154°, although the absolute cross sections are 30–50 % larger at the higher energy.

In Fig. 3 we show the charge distributions for each target observed at 12°, where nonequilibrium emission dominates, and at 160°, where equilibrium emission is most probable. The probability for emission of IMFs from the neutron-excess ^{124}Sn target is significantly less than for the ^{116}Sn target. This effect is more pronounced at the backward angle and for larger Z fragments. The ratio of the cross sections (^{116}Sn/^{124}Sn) ranges from 1.03 (lithium) to 3.3 (neon) at 12°, and from 1.6 to 3.6 at 160°. The backward-angle distributions can be approximated by a power law [21], $\sigma(Z)\alpha Z^{-\tau}$, dependence with a τ parameter of 3.3 and 4.0 for ^{116}Sn and ^{124}Sn targets, respectively. For the forward-angle distributions, the values of the power-law parameter are 5.2 and 5.6. However, in this case better fits can be obtained using an exponential function $\sim \exp(-\alpha Z)$ with $\alpha(^{116}\text{Sn}) = 0.98$ and $\alpha(^{124}\text{Sn}) = 1.13$.

In Fig. 4 the fractional isotopic yields for each element observed at the backward angle (154°) are shown by his-

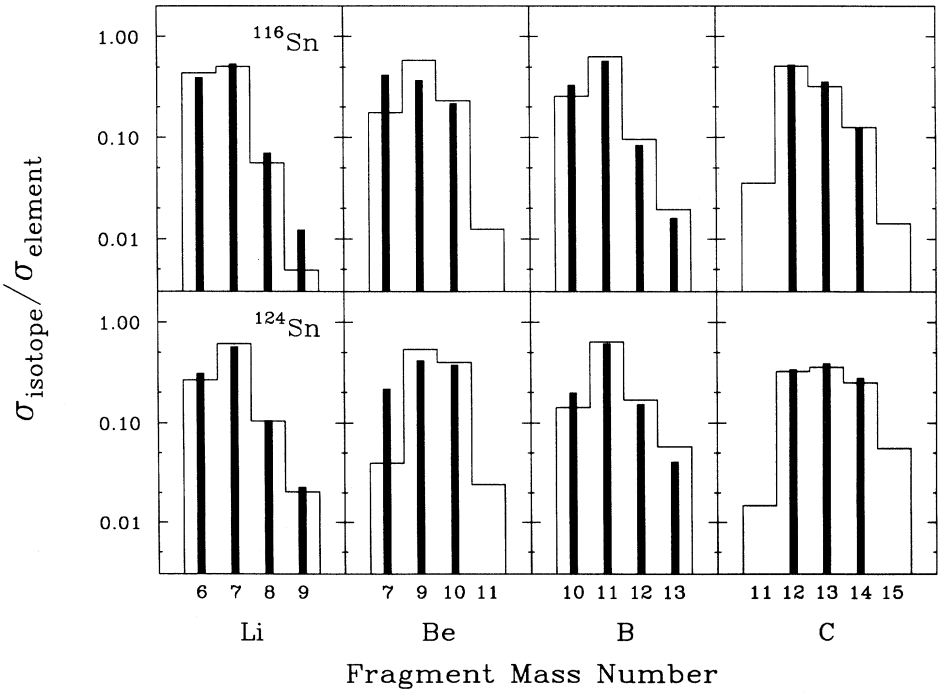

FIG. 4. Isotopic yields as a fraction of the elemental cross section at 154° (histograms). Solid bars show the isotopic ratios for the nonequilibrium IMF component. Upper set is for ^{116}Sn target; lower set is for ^{124}Sn.

TABLE I. Elemental cross sections for $Z=3-10$ fragments from ^{116}Sn and ^{124}Sn targets.

Z	σ (mb) ^{116}Sn	^{124}Sn
3	14.0±1.6	12.9±1.6
4	2.8±0.4	2.3±0.3
5	1.5±0.2	0.99±0.12
6	0.90±0.11	0.41±0.06
7	0.28±0.04	0.12±0.02
8	0.15±0.02	0.057±0.10
9	0.063±0.010	0.025±0.005
10	0.055±0.010	0.016±0.003

tograms. These products are attributed to equilibrium emission and assumed to be emitted isotropically [3]. The nonequilibrium component at forward angles is represented by solid bars. In this case the differential cross sections were integrated over angle after subtracting the equilibrium component. Data for ^{11}Be and ^{15}C fragments are excluded because of insufficient statistics. Two general features are apparent in these plots. First, the relative intensity of neutron-excess isotopes is higher in the case of the neutron-rich ^{124}Sn target as compared to ^{116}Sn. Second, there is a tendency for the most neutron-deficient isotopes to be enhanced in the nonequilibrium yields relative to the equilibrium component for $Z=3-5$ IMFs (^{6}Li from ^{116}Sn being the one exception). This effect is particularly strong for the proton-excess isotope ^{7}Be. Similar forward-angle enhancement has been observed for ^{3}He yields in 270 MeV ^{3}He-induced reactions [22] and for ^{11}C in heavy-ion-induced reactions [13]. Since some fraction of the observed products may come from the decay of particle-unstable states, these relative yields cannot be interpreted directly. Nonetheless, the overall trends suggest a picture in which N/Z equilibration in the average nonequilibrium source has evolved to a lesser degree than that of the equilibrium source. Alternatively, the nonequilibrium IMFs may be emitted in a higher state of excitation and subsequently decay toward $N=Z$ products. Both explanations suggest emission on a shorter time scale for nonequilibrium fragments, consistent with the strongly forward-peaked angular distributions (Fig. 2).

Figure 5 shows the ratio of the cross section for the ^{116}Sn target to that for the ^{124}Sn target, plotted as a function of the fragment mass number of Li, Be, B, and C isotopes. The diamonds (upper part) and the circles (lower part) represent the angle-integrated nonequilibrium and the equilibrium components, respectively. The relation between the cross-section ratios for the two targets can be described by an exponential function:

$$\sigma(^{116}\mathrm{Sn})/\sigma(^{124}\mathrm{Sn}) \approx \exp(-\gamma A_{\mathrm{IMF}}) . \quad (2)$$

The lines in Fig. 5 are fits to the data using the above relationship. Values of the parameter γ are shown on the plots and in Table II. As can be seen, the slopes for the equilibriumlike IMFs are nearly constant for each element. The average value of the γ parameter is 0.59. For the nonequilibrium component, the slope progressively increases with the increasing fragment atomic number. The corresponding values of the slope parameter change

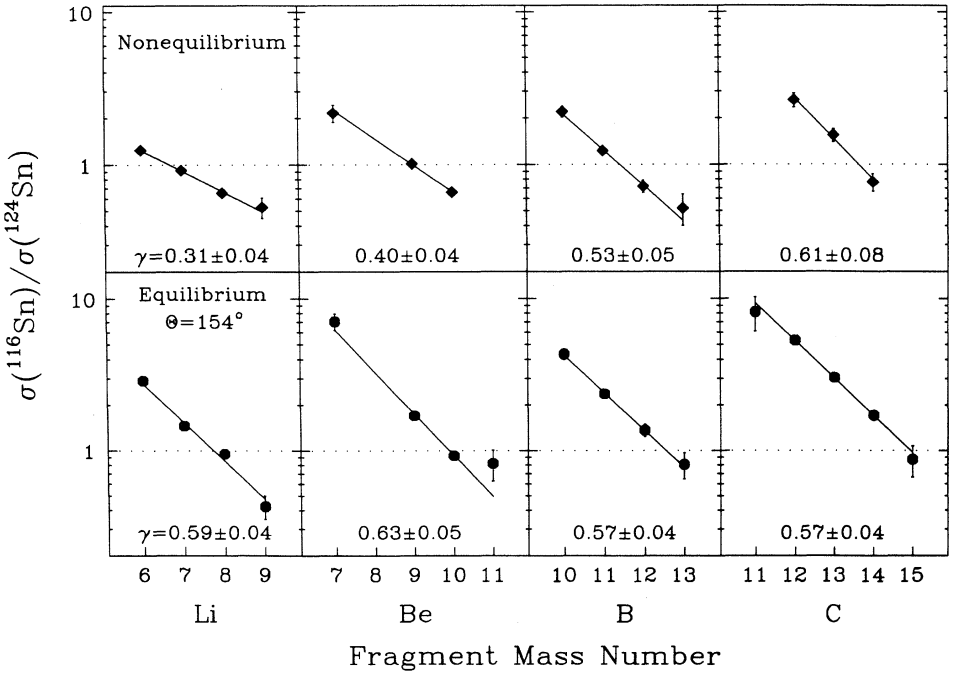

FIG. 5. Ratio of yield for a given isotope from ^{116}Sn target to that from ^{124}Sn target as a function of mass number of Li, Be, B, and C, as indicated on figure. Upper set represents nonequilibrium data at forward angles; lower set is for data obtained at 154°. Line is fit to data with Eq. (2); slope parameter for each element is given in Table II.

TABLE II. Exponential slope parameters for isotopic distributions.

Element	Slope parameter Nonequilibrium	Equilibrium
Li	0.31±0.04	0.59±0.04
Be	0.40±0.04	0.63±0.05
B	0.53±0.05	0.57±0.04
C	0.61±0.08	0.57±0.04

from 0.31 for lithium to 0.61 for carbon; i.e., for the lighter elements, the composition of the isotopic yields differs significantly for equilibrium and nonequilibrium components, whereas for carbon both components exhibit similar slopes. Note, however, that the absolute cross-section ratios are quite different for the two mechanisms.

In Fig. 6 isotope ratios are plotted as a function of IMF kinetic energy for Li, Be, B, and C fragments at 12° and 154° for the ^{124}Sn target. The isotope ratio is defined here as the yield of a given isotope relative to the total element yield. Again, the forward-angle data emphasize nonequilibrium emission whereas the backward-angle data are representative of equilibrated decay. The isotopic ratios for the ^{116}Sn target are similar to ^{124}Sn, although the relative yields of the heavier isotopes of each element are reduced, as reflected in Figs. 4 and 5. For Li and Be fragments emitted at forward angles, the probability for emission of neutron-excess isotopes clearly decreases as a function of increasing fragment energy. The same, but weaker, behavior is present for boron isotopes and for carbon it is barely discernible. Similar observations have been reported previously [14]. For emission at backward angles, where the IMF kinetic-energy scale is greatly compressed, there is little evidence for a dependence of the isotope ratio on fragment kinetic energy, consistent with expectations for an equilibrated system.

IV. INTERPRETATION OF RESULTS

A. Statistical calculations

The backward-angle emission of IMFs can be interpreted in terms of statistical emission from a compound nucleus [2,3,5–7]. In an effort to describe the backward-angle isotope distributions in terms of emission barriers, a schematic statistical calculation has been performed and normalized to the data. As an initial condition, an excitation energy based on full momentum transfer and a zero angular momentum approximation has been employed. The former assumption overestimates the excitation energy; coincidence studies have shown that on average only about 80% of full momentum transfer is achieved when IMFs are emitted in similar reactions [23]. Decreasing the input excitation energy will produce steeper IMF charge distributions. The zero angular momentum assumption has the reverse effect; i.e., inclusion of angular momentum serves to flatten the charge distribution.

We assume initially that light fragments are emitted in their ground states. For each isotope the decay width is calculated using the formula of Swiatecki [24], and then multiplied by $2J+1$, where J is the ground-state spin of the light fragment. The level density of the activated complex is determined by the excited residual nucleus, for which a level-density parameter of $A/8.5$ MeV^{-1} was assumed.

In calculating the decay barrier heights B for very asymmetric mass division of a compound nucleus of $A \simeq 120$, the deformation of fragments can be neglected [25]. Thus, the decay barrier height is given as the sum

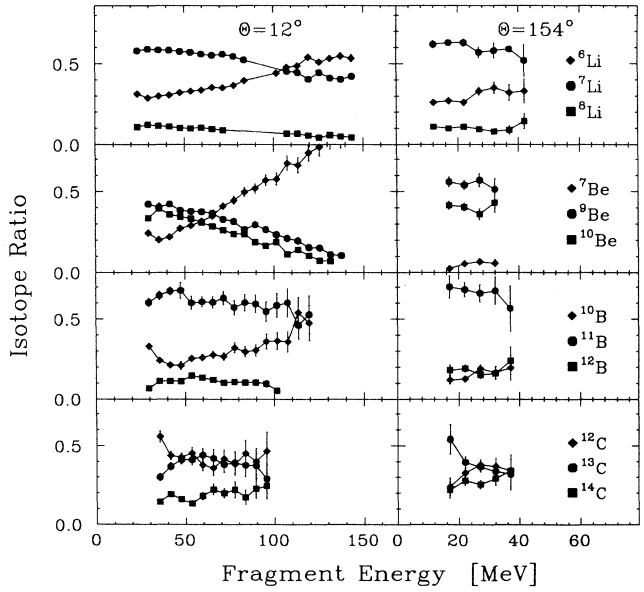

FIG. 6. Isotope ratios [fraction of given isotope to total elemental yield, $\sigma(Z,A)/\sigma(Z)$] as a function of IMF kinetic energy for Li, Be, B, and C ejectiles from ^{124}Sn target. Left column is for data at 12°; right column for data at 154°.

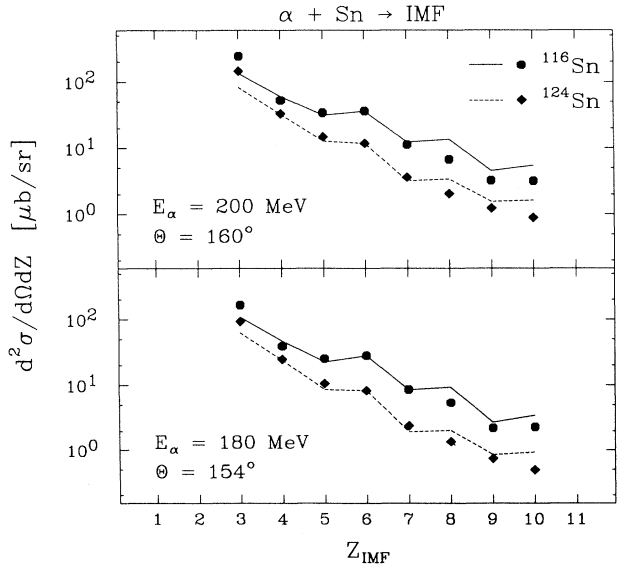

FIG. 7. Charge distributions for IMFs emitted from ^{116}Sn and ^{124}Sn targets at 160° (200 MeV ^{4}He beam; upper frame) and 154° (180 MeV ^{4}He beam; lower frame). Solid and dashed lines are statistical-model estimates described in Sec. IV A.

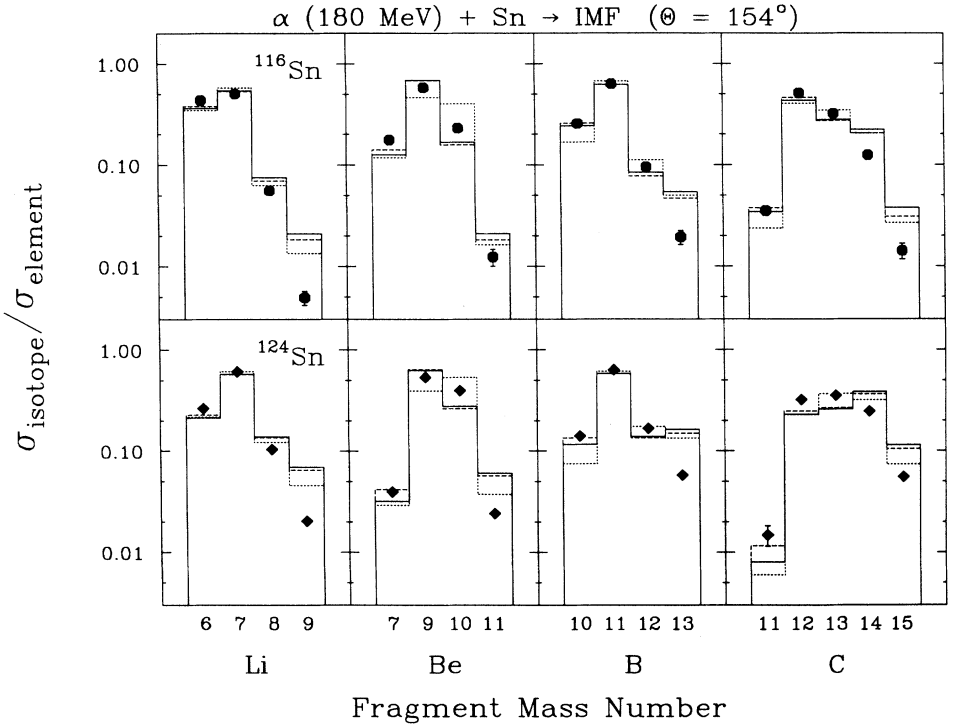

FIG. 8. Isotopic distributions for Li, Be, B, and C ejectiles at 154° from ^{116}Sn (upper) and ^{124}Sn (lower) targets. Solid histogram is the result of statistical calculations described in Sec. IV A; dashed histogram shows approximation of Eq. (3), and dotted histogram includes population of excited states for fragments. Data are given by closed points.

of the separation energy and the fragment-fragment potential at the radius of the barrier. We have used here the experimental IMF mass [26], the droplet-model masses of the residual and compound nuclei without shell corrections [27], the proximity potential [28], and the *s*-wave fusion barrier radius [29].

In Fig. 7 the measured (points) and calculated (lines) for the Z distributions are compared. The calculated yields are normalized to the $Z=6$ data. This simple model reproduces the backward-angle charge distributions relatively well, although there is a tendency to underpredict Li yields and to overpredict heavier fragment production. Isotopic predictions are shown in Fig. 8 by the solid histograms. The dashed histograms present results of the calculation, in which the decay width was taken as

$$\Gamma \sim (2J+1)\exp(-B/T) , \tag{3}$$

with a constant temperature of $T=3.2$ MeV for all isotopes and for both targets. This value is the average temperature calculated for the residual nuclei produced in these decays. This simplification does not change the results appreciably and is used in further calculations.

The qualitative features of the IMF isotopic composition are reproduced; however, the model overpredicts yields for neutron-excess fragments. This discrepancy can be understood as a consequence of the assumption that only the ground states of emitted fragments are important, whereas the population of excited states may play an important role. To estimate this effect, we have

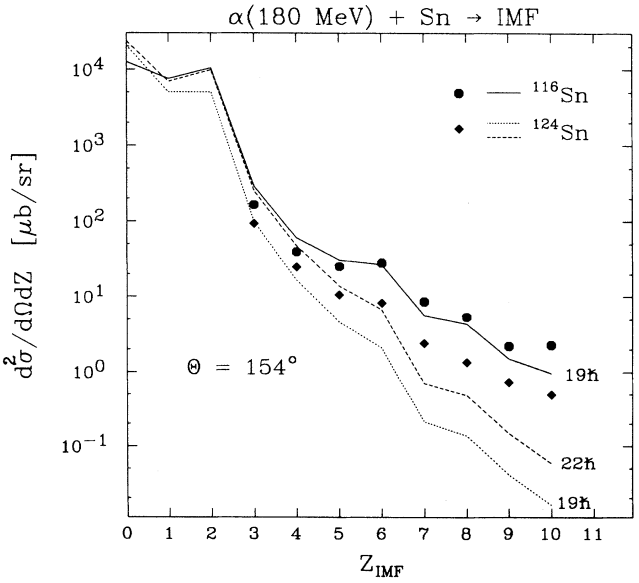

FIG. 9. Charge distributions for IMFs emitted at 154° for 180 MeV ^{4}He + ^{116,124}Sn reactions, compared with BUSCO [30] calculation. Calculations are performed for $L=19\hbar$ for both systems and $L=22\hbar$ for ^{124}Sn.

also performed calculations which include excited states. A Boltzmann population of states, a constant temperature of $T=3.2$ MeV, and no feeding from decays of $Z \geq 7$ fragments were assumed in these calculations. The result is shown in Fig. 8 by the dotted histograms. Somewhat lower intensities of the most neutron-excess and the most neutron-deficient isotopes are predicted relative to those from the ground-state calculations.

Empirically, the yields can be described quite well using the results of Fig. 5, where the experimental ratios $\sigma(^{116}\mathrm{Sn})/\sigma(^{124}\mathrm{Sn})$ can be approximated by an exponential function of the fragment mass number [see Eq. (2)]. Using the decay width formula of Eq. (3), we obtain

$$\sigma(^{116}\mathrm{Sn})/\sigma(^{124}\mathrm{Sn}) \approx \exp\{-[B(^{116}\mathrm{Sn})-B(^{124}\mathrm{Sn})]/T\} . \quad (4)$$

With good accuracy, the difference $B(^{116}\mathrm{Sn})-B(^{124}\mathrm{Sn})$ calculated from Ref. [24] can be parametrized by a linear function of the fragment mass number,

$$B(^{116}\mathrm{Sn})-B(^{124}\mathrm{Sn})=C(Z_F)+1.9A_F \ (\mathrm{MeV}) \quad (5)$$

where $C(Z_F)$ is a constant for each Z value. Combining this equation with Eq. (4), we find

$$\sigma(^{116}\mathrm{Sn})/\sigma(^{124}\mathrm{Sn}) \sim \exp(-\gamma A_F) , \quad (6)$$

where $\gamma=1.9$ MeV/T. The average experimental value of the γ parameter for the Li, Be, B, and C fragments (Fig. 5, lower part) is 0.59 ± 0.04, corresponding to the emission temperature in the range 3.0–3.4 MeV, consistent with the temperature expected for residual nuclei formed in these reactions.

In order to examine the additional influence of neutron binding energies and angular momentum on the ^{116,124}Sn charge distributions, we have also performed calculations with the evaporation code BUSCO [30]. These results are shown in Fig. 9. Using a value of $L=19\hbar$ and the maximum available excitation energy, the cross sections for the ^{116}Sn target are relatively well reproduced. For the ^{124}Sn target the calculation successfully predicts the lower IMF cross sections relative to ^{116}Sn, but is much less successful in describing the heaviest fragment yields. In both cases the slope of the calculation is much steeper than the data. By increasing the input angular momentum to $L=22\hbar$, a somewhat better fit to the ^{124}Sn data is obtained, both in magnitude and slope. A possible explanation for this result is that the L-wave distribution for the average emitting system formed in the ^{4}He + ^{124}Sn reaction may sample a higher range of angular momentum values than for ^{4}He + ^{116}Sn reactions, a result consistent with the increased decay widths for neutron emission from the neutron-excess system. Nonetheless, the BUSCO calculation underpredicts heavy fragment yields relative to the statistical calculations above, especially for neutron-excess systems. This suggests that calculations of $\Gamma_n/\Gamma_{\mathrm{IMF}}$ in this code may need some modification.

While the backward-angle emission of IMFs can be understood relatively well in terms of the decay of a compound nucleus, the mechanism of nonequilibrium production is still poorly understood. For these ejectiles the important question of the time scales complicates the theoretical interpretation of the data. Recent measurements [5,11] indicate that isotopic ratios observed at for-

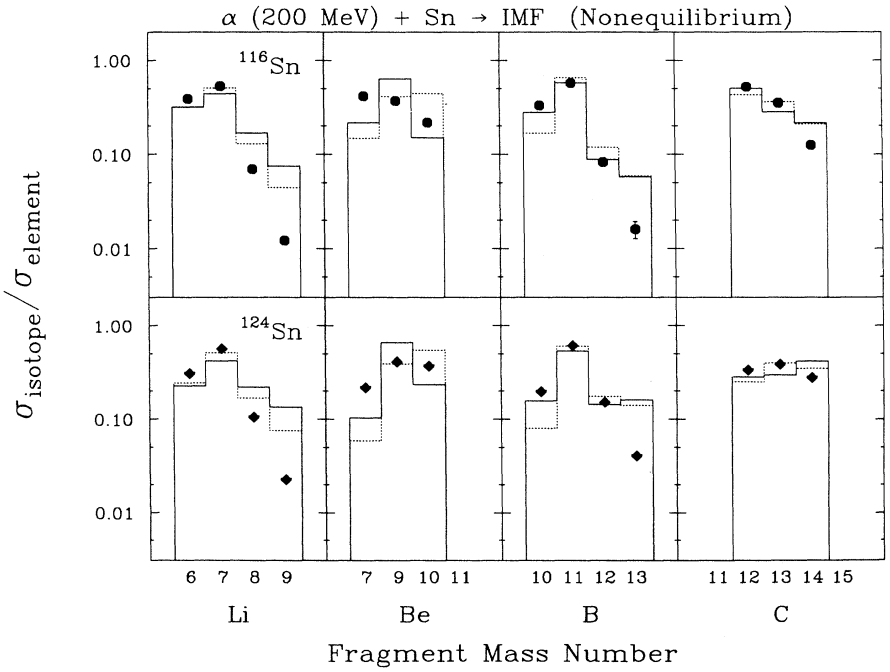

FIG. 10. Isotopic distributions for Li, Be, B, and C IMFs observed at forward angles for ^{116}Sn (upper) and ^{124}Sn (lower) targets. Histograms are results of calculations described in Sec. IV A. Solid line is for ground state only; dotted line includes excited states of fragments.

ward angles can be interpreted in terms of partial statistical equilibrium of a composite system involving most of the projectile-target system.

If we assume local N/Z equilibration, we can calculate the relative isotopic intensities for nonequilibrium IMFs in the same manner as for equilibrated emission. In this case, the effective level-density parameter may have different values for different exit channels. We assume a constant effective temperature for all isotopes of a given element for both targets. Using the values of the slope parameters given in Fig. 5 and Eq. (6), we find the following effective temperatures: 6.1±0.8 MeV (Li), 4.8±0.5 MeV (Be), 3.6±0.4 MeV (B), and 3.1±0.4 MeV (C). Thus, the apparent emission temperatures systematically decrease with increasing fragment atomic number, in qualitative agreement with predictions of the accreting source model [31,32]. The isotopic composition calculated for these temperatures is shown in Fig. 10 by solid histograms (ground states only), and by dotted histograms (excited states included). Also in this case the yields are overestimated for neutron-excess fragments; however, the qualitative trends are reproduced except for Be isotopes.

B. Accreting source calculations

The accreting source model [16,31,32] is based on the assumption of local statistical emission from an excited subsystem of the nucleus created by the fusion of the projectile with some number of target nucleons. This source simultaneously emits fragments and cools by accreting nucleons from the remainder of the target. In our calculations we have assumed an initial source size of eight nucleons, accretion rate of 2 nucleons/fm c, and exit-channel Coulomb barrier of 0.9 times the touching-sphere value [16]. The Fermi energy of 24 MeV and normalization coefficients were fixed by requiring a fit to the charge distributions. In Fig. 11, the model predictions

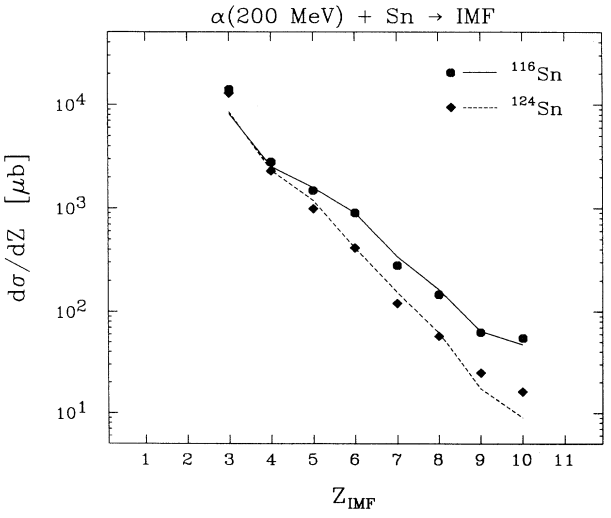

FIG. 11. Total charge distribution for IMFs emitted from ^{116}Sn and ^{124}Sn, as indicated on figure. Fits are predictions of accreting source model [16,31]. Experimental cross sections are tabulated in Table I.

are compared with the total cross sections which include both nonequilibrium and equilibriumlike components.

The isotopic yield results are shown in Fig. 12. We observed general agreement with the data, including ^{7}Be, for which the previous calculations were unsuccessful. As can be seen in the upper part of Fig. 13, the ratios $\sigma(^{116}\text{Sn})/\sigma(^{124}\text{Sn})$ are also reasonably well reproduced by the calculations (solid lines). In the lower part of this figure solid bars show the average emission temperature calculated from the accreting source model for the ^{116}Sn target; dotted bars are for the ^{124}Sn target. In general, the temperatures are lower for heavier fragments and somewhat higher in the case of the ^{124}Sn target.

Whereas the calculation reproduces the total cross sections well, it fails to reproduce the angular distributions (Fig. 2). The predicted angular distributions are much flatter than the experimental ones. Also, the slopes of the energy spectra for the lighter fragments are too steep. For the heavier fragments, the spectral shapes are well reproduced, although the absolute cross sections are too small at forward angles.

Somewhat more rapidly decreasing angular distributions can be obtained by using a lower value of the accretion rate. The charge and isotopic distributions, as well as energy spectra, are relatively insensitive to such a change. To obtain flatter energy spectra, however, it is necessary to increase the Fermi energy, which in turn causes the charge and isotopic distributions to become flatter. Thus, the accreting source model describes many features of these data satisfactorily, although complete self-consistency cannot be achieved for all observables.

V. CONCLUSIONS

The effect of target N/Z ratio on the properties of IMF ejectiles has been investigated in the reaction of $E/A \approx 50$ MeV ^{4}He ions with targets of ^{116}Sn and ^{124}Sn. Both equilibriumlike and nonequilibrium sources have been studied by performing measurements at extreme backward and forward angles.

The data demonstrate the influence of target composition on both the charge and isotopic distributions of the fragments. Elemental cross sections from the ^{4}He + ^{116}Sn system are distinctly enhanced relative to ^{4}He + ^{124}Sn. This effect is strongest for the equilibriumlike fragments, where the yields are 2–3 times larger for ^{116}Sn compared to ^{124}Sn. For nonequilibrium emission, both targets produce similar yields for light IMFs; however, the ratio of the elemental cross sections from ^{116}Sn to those from ^{124}Sn becomes increasingly larger as a function of increasing fragment charge. This result is interpreted in terms of the higher conditional barriers and lower average neutron binding energies for the ^{4}He + ^{124}Sn system, thereby favoring decay via neutron emission at the expense of IMF probability.

For a given element the ratio of the IMF cross section from the ^{116}Sn system to that from ^{124}Sn for any series of isotopes is found to decrease with increasing neutron number. This behavior reflects the larger N/Z ratio of the composite system formed from ^{124}Sn and can be described in terms of a simple exponential function related

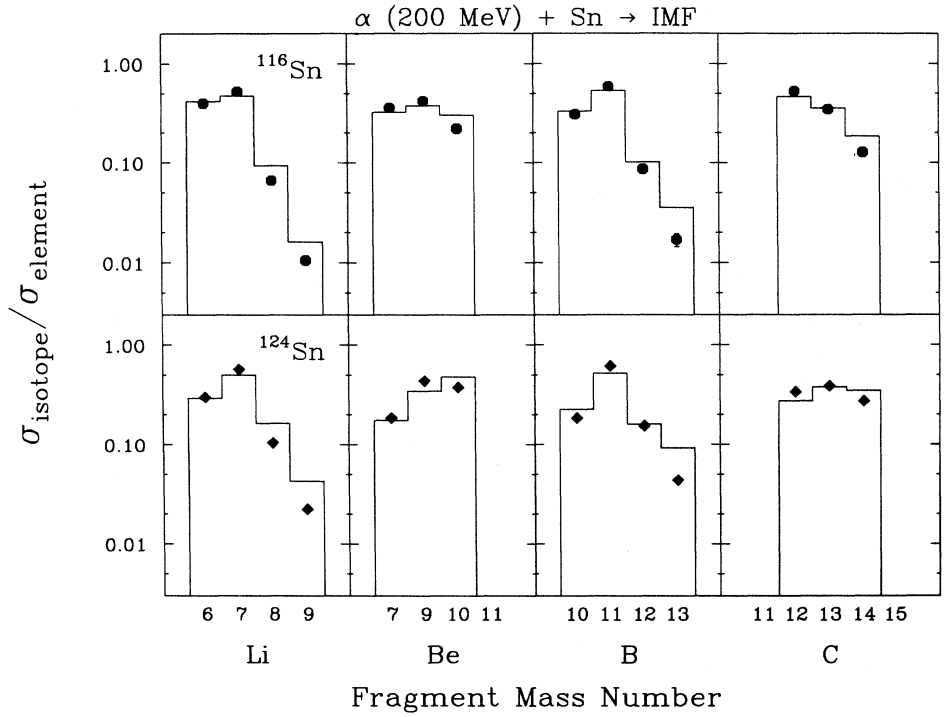

FIG. 12. Isotopic ratios for Li, Be, B, and C fragments, for ^{116}Sn (upper) and ^{124}Sn (lower) targets. Solid line is the prediction of accreting source model [16,31].

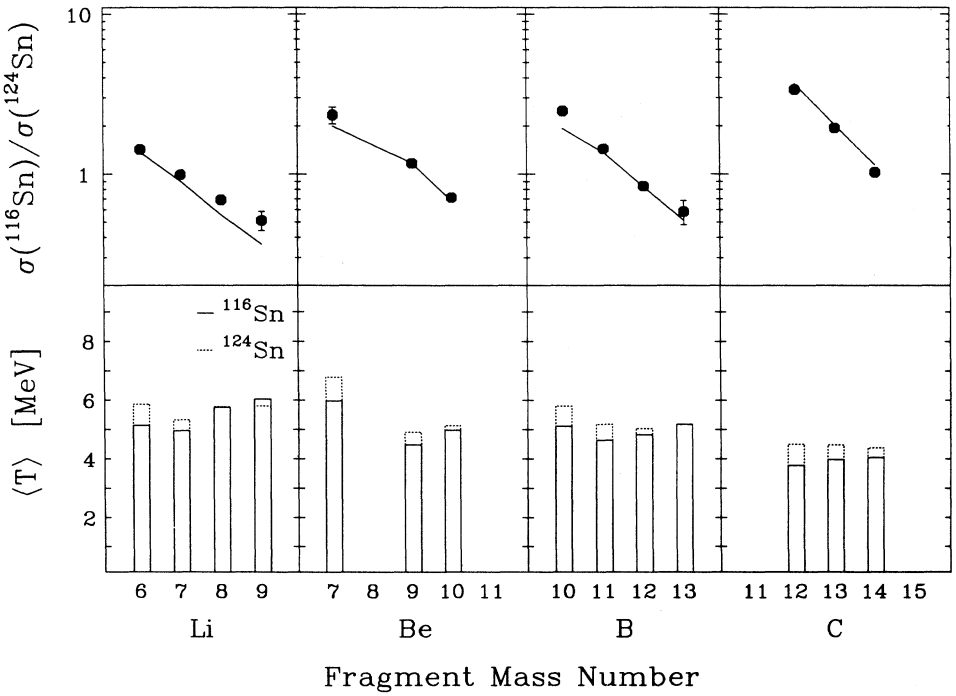

FIG. 13. Top: ratio of nuclidic yield of IMFs from ^{116}Sn to ^{124}Sn. Solid line is the prediction of accreting source model [16,31]. Bottom: predicted average emission temperature, $\langle T \rangle$, for Li, Be, B, and C; solid histograms are for ^{116}Sn target and dots are for ^{124}Sn.

to conditional barrier differences. This isotopic dependence on target N/Z is strongest for the backward-angle component of the spectra and the slope of the ratio $\sigma(^{116}\mathrm{Sn})/\sigma(^{124}\mathrm{Sn})$ is the same for Li, Be, B, and C ejectiles. Such behavior is consistent with emission from an equilibrated system.

At forward angles the nuclidic yields are found to be sensitive to both the N/Z of the target and the ejectile. Neutron-excess IMFs are favored with the ^{124}Sn target; however, the exponential slope of the ratio $\sigma(^{116}\mathrm{Sn})/\sigma(^{124}\mathrm{Sn})$ for the isotopes of a given element evolve from a rather flat behavior for $Z=3$ isotopes to one for $Z=6$ that is virtually identical to that for equilibriumlike emission. Thus, nonequilibrium emission of light IMFs appears to be less sensitive to the target-projectile composition, possibly indicating that only partial N/Z equilibration is achieved for these products. Another feature of the forward-angle spectra is that the isotope ratios depend on IMF kinetic energy. Near the Coulomb peak, the isotopic ratios at forward angles are similar to those at backward angles. However, for increasingly energetic IMFs, the yield of neutron-deficient isotopes is enhanced with respect to the heavier isotopes. This effect is strongest for Li and Be isotopes.

A simple statistical-model calculation which includes excited states of the fragments gives fair agreement when normalized to the backward-angle data. In general, there is a tendency for the calculation to overpredict the yields of neutron-excess fragments. The evaporation code BUSCO, which also takes neutron binding energies and angular momentum into account, predicts the observed elemental cross-section differences between the ^{116}Sn systems on an absolute scale. However, these calculations emphasize the importance of an accurate knowledge of the angular momentum distribution of the emitting system, which can influence $\Gamma_n/\Gamma_{\mathrm{IMF}}$ strongly. An accreting source calculation, calibrated by the charge distributions, also provides a reasonable description of the nuclidic yield results for the entire data set. However, this calculation encounters difficulties in fitting spectral shapes at forward angles, as well as angular distributions.

ACKNOWLEDGMENTS

The authors acknowledge the assistance of W. Lozowski in preparing the separated-isotope ^{116}Sn and ^{124}Sn targets. This research was supported by the U.S. Department of Energy and the National Science Foundation.

[1] R. E. L. Green and R. G. Korteling, Phys. Rev. C **22**, 1594 (1980); R. E. L. Green, R. G. Korteling, and K. P. Jackson, *ibid.* **29**, 1806 (1984).
[2] L. G. Sobotka, M. L. Padgett, G. J. Wozniak, G. Guarino, A. J. Pacheco, L. G. Moretto, Y. Chan, R. G. Stokstad, I. Tserruya, and S. Wald, Phys. Rev. Lett. **51**, 2187 (1983).
[3] K. Kwiatkowski, J. Bashkin, H. Karwowski, M. Fatyga, and V. E. Viola, Phys. Lett. B **171**, 41 (1986).
[4] N. T. Porile *et al.*, Phys. Rev. C **39**, 1914 (1989).
[5] W. Trautmann *et al.*, Nucl. Phys. **A471**, 191c (1987).
[6] J. L. Wile *et al.*, Phys. Rev. C **45**, 2300 (1992).
[7] N. M. Papadakis *et al.*, Phys. Lett. B **240**, 317 (1990).
[8] V. E. Viola and K. Kwiatkowski, in *Proceedings of the Symposium: Towards a Unified Picture of Nuclear Dynamics,* AIP Conf. Proc. No. 250, edited by S. M. Lee and F. Sakata (AIP, New York, 1991).
[9] Y. D. Kim *et al.*, Phys. Rev. Lett. **63**, 494 (1989).
[10] W. Trautman, in *Proceedings of the Symposium: Towards a Unified Picture of Nuclear Dynamics,* AIP Conf. Proc. No. 250, edited by S. M. Lee and F. Sakata (AIP, New York, 1991).
[11] R. Wada *et al.*, Phys. Rev. Lett. **58**, 1829 (1987).
[12] F. Deak, A. Kiss, Z. Seres, A. Galonsky, L. Heilbroun, and H. R. Schelin, Phys. Rev. C **42**, 1029 (1990).
[13] V. E. Viola and K. Kwiatkowski, in *Proceedings of the XIIIth Symposium on Nuclear Physics,* edited by C. Chavez-Lomeli (World Scientific, Singapore, 1990), p. 245.
[14] E. Renshaw, S. J. Yennello, K. Kwiatkowski, R. Planeta, L. W. Woo, and V. E. Viola, Phys. Rev. C **44**, 2618 (1991).
[15] V. V. Ardeichikov *et al.*, Yad. Fiz. **98**, 1736 (1988) [Sov. J. Nucl. Phys. **48**, 1043 (1988)].
[16] D. J. Fields, W. G. Lynch, C. B. Chitwood, C. K. Gelbke, M. B. Tsang, H. Utsonomiya, and J. Aichelin, Phys. Rev. C **30**, 1912 (1984).
[17] H. W. Barz, H. Schulz, J. P. Bondorf, J. Lopez, and K. Sneppen, Phys. Lett. B **211**, 10 (1988).
[18] K. Kwiatkowski, K. Komisarcik, J. L. Wile, S. J. Yennello, D. E. Fields, V. E. Viola, and B. G. Glagola, Nucl. Instrum. Methods **299**, 166 (1990).
[19] W. G. Meyer, University of Maryland, 1978 (unpublished program).
[20] N. R. Yoder, IUCF Internal Report No. 85-4, 1985 (unpublished); C. R. Gould and N. R. Roberson, IEEE Trans. Nucl. Soc. **NS-30**, 3758 (1985).
[21] J. E. Finn *et al.*, Phys. Rev. Lett. **49**, 1321 (1982).
[22] W. Skulski, M. Fatyga, H. J. Karwowski, K. Kwiatkowski, V. E. Viola, and K. Hicks, Phys. Rev. C **40**, 1279 (1989).
[23] M. Fatyga, R. C. Byrd, K. Kwiatkowski, V. E. Viola, W. G. Wilson, L. W. Woo, H. J. Karwowski, J. Jastrzebski, and W. Skulski, Phys. Lett. B **185**, 321 (1987).
[24] W. J. Swiatecki, Aust. J. Phys. **36**, 641 (1983).
[25] J. Brzychczyk and J. Łukasik, Nucl. Phys. **A535**, 272 (1991).
[26] A. H. Wapstra and K. Bos, At. Data Nucl. Data Tables **19**, 177 (1977).
[27] W. D. Myers, At. Data Nucl. Data Tables **17**, 411 (1976).
[28] J. Błocki, J. Randrup, W. J. Swiatecki, and C. F. Tsang, Ann. Phys. (N.Y.) **105**, 427 (1977).
[29] W. W. Wilcke, J. R. Birkelund, H. J. Wollersheim, A. D. Hoover, J. R. Huizenga, W. U. Schröder, and L. E. Tubbs, At. Data Nucl. Data Tables **25**, 389 (1980).
[30] J. Gomez de Campo, Phys. Rev. Lett. **61**, 290 (1988).
[31] W. A. Friedman and W. G. Lynch, Phys. Rev. C **28**, 16, 950 (1983).
[32] B. Jakobsson, L. Karlsson, and J. Lopez, Nucl. Phys. **A531**, 143 (1991).